

LETTER TO THE EDITOR

Cold and warm molecular gas in the outflow of 4C12.50

K. M. Dasyra¹ and F. Combes¹

Observatoire de Paris, LERMA (CNRS:UMR8112), 61 Av. de l'Observatoire, F-75014, Paris, France

ABSTRACT

We present deep observations of the ^{12}CO (1-0) and (3-2) lines in 4C12.50, carried out with the 30 m telescope of the Institut de Radioastronomie Millimétrique. Our observations revealed the cold molecular gas component of a warm molecular gas outflow that was previously known from *Spitzer* space telescope data. The ^{12}CO (3-2) profile indicates the presence of absorption at -950 km s^{-1} from systemic velocity with a central optical depth of 0.22. Its profile is similar to that of the HI absorption that was seen in radio data of this source. A potential detection of the (0 \rightarrow 1) absorption enabled us to place an upper limit of 0.03 on its central optical depth, and to constrain the excitation temperature of the outflowing CO gas to $\geq 65\text{ K}$ assuming that the gas is thermalized. If the molecular clouds are fully obscuring their background millimeter continuum that is emitted by the radio core, the H_2 column density is $\geq 1.8 \times 10^{22}\text{ cm}^{-2}$. The outflow is then carrying an estimated cold H_2 mass of at least $4.2 \times 10^3 M_\odot$ along the nuclear line of sight. This mass will be even higher when integrated over several lines of sight, but if it were to exceed $3 \times 10^9 M_\odot$, the outflow would most likely be seen in emission. Since the ambient cold gas reservoir of 4C12.50 is $1.0 \times 10^{10} M_\odot$, the outflowing-to-ambient mass ratio of the warm gas (37%) could be elevated with respect to that of the cold gas.

Key words. ISM: jets and outflows — ISM: kinematics and dynamics — Line: profiles — Galaxies: active — Galaxies: nuclei — Infrared: galaxies

1. Introduction

Through jets, winds, and radiation pressure, active galactic nuclei (AGN) can affect the collapse of their surrounding molecular gas and the formation of new stars in the galaxies in which they reside. While simulations attribute a considerable (if not great) role in AGN feedback shaping galaxy properties (e.g., Croton et al., 2006; Sijacki et al., 2007; Booth & Schaye, 2009; Hopkins & Elvis, 2010; Debuhr et al., 2012), the question remains open from an observational point of view. Are AGN-driven outflows that suppress star formation frequent enough to affect the observed luminosity and mass functions of galaxies? To answer this question, not only do we need to identify objects with massive, AGN-driven outflows of molecular gas, but to also examine and take into account the outflow effects on the different phases of this gas.

Various phases of an AGN-driven molecular gas outflow have so far been observed in the nearby ultraluminous infrared galaxy (ULIRG) Mrk231. Plateau de Bure interferometric observations showed that the outflowing CO, with a corresponding cold H_2 mass of $6 \times 10^8 M_\odot$ and a flow rate of $700 M_\odot\text{ yr}^{-1}$, is capable of suppressing star formation (Feruglio et al., 2010). Aalto et al. (2012) recently discovered the dense ($\gtrsim 10^4\text{ cm}^{-3}$) component of this outflow from broad HCN(1-0) line profile wings. The OH mass content in the outflow exceeds $7 \times 10^8 M_\odot$ based on profile fitting of the $79\text{ }\mu\text{m}$ and $199\text{ }\mu\text{m}$ lines seen with *Herschel* (Fischer et al., 2010), leading to a total of more than $10^9 M_\odot$ of molecules in the wind.

Another straightforward and quantitative comparison that has yet to be performed is that between the warm

and the cold H_2 gas mass in the outflow vs the rest of the interstellar medium. The only source that is suitable for this analysis, i.e., the only source that is known to have a massive outflow of its few hundred Kelvin gas, as seen from mid-infrared H_2 rotational line profiles (Dasyra & Combes, 2011), is 4C12.50. In this letter, we present evidence for the existence of cold molecules in its outflow, and we evaluate the relative amount of warm and cold gas that the AGN feedback kinematically distorts. We adopt $\text{H}_0=70\text{ km s}^{-1}\text{ Mpc}^{-1}$, $\Omega_M=0.3$, and $\Omega_\Lambda=0.7$ throughout.

2. Data acquisition and reduction

The observations were carried out with the 30 m telescope of the Institut de Radioastronomie Millimétrique between December 21–22 2011, and on January 1 2012 as part of the program 235-11. For the ^{12}CO (1-0) observations, EMIR was tuned to 102.700 GHz. For the ^{12}CO (3-2) observations, the receivers were tuned to 308.086 GHz during the first observing run and to 308.600 GHz during the second observing run, to ensure that the observed line properties are not affected by potential standing waves, atmospheric line residuals, or bad channels. Parallel to the CO observations, we carried out HCN and HCO^+ (2-1) observations with a common tuning of 158.427 GHz. Both the FTS and WILMA backends, with corresponding resolutions of 0.2 MHz and 2 MHz, were simultaneously used as backends to allow consistency checks. The inner and the outer parts of the FTS were used, enabling us to better sample the continuum near each line. Wobbler switching mode with a throw of $80''$ and 0.65 seconds per phase was used for fast sampling of the continuum. The telescope pointing accuracy

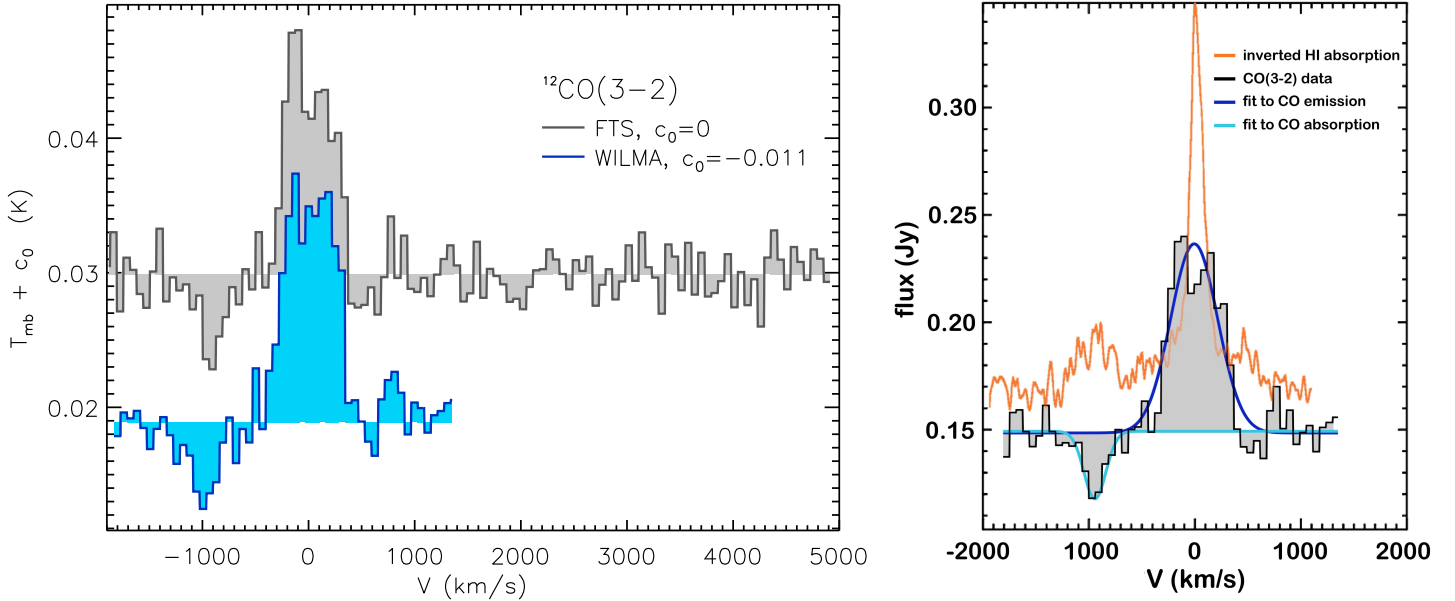


Fig. 1. *Left:* Individual FTS and WILMA spectra of $^{12}\text{CO}(3-2)$ in 4C12.50, binned to 62 km s^{-1} channels and shifted by a constant c_0 , when needed. Both spectra indicate an absorption feature at approximately -1000 km s^{-1} . *Right:* Flux-calibrated line profile of $^{12}\text{CO}(3-2)$. To be least affected by potential artifacts, the profile presented in this panel is the average of the WILMA and the FTS data. Gaussian functions with parameters that best fit the emission component at systemic velocity and the absorption component at -950 km s^{-1} are shown in blue and cyan, respectively. The inverted HI absorption that is seen in the radio data of 4C12.50 (Morganti et al., 2004) is overplotted in orange for an arbitrary scale and continuum level.

was of $2''$, and the system temperature varied from 310 to 580 K at 1 mm during our observations.

To reduce the 1 mm data, we first removed bad channels from all individual scans. The three parts of each FTS scan, corresponding to the output of a different spectrometer, were fitted with linear baselines and brought to the same continuum level, i.e. to the median value of the full scan. This step was performed to ensure that there is no continuum discontinuity between the three parts that could introduce artificial features to the combined spectrum. We averaged the individual scans of each frequency tuning and backend, discarding scans with unstable baselines. The inner and the outer FTS spectra were then stitched together. For each backend, the spectra of the two frequency tunings were brought to a common reference frequency of 308.245 GHz, where the $^{12}\text{CO}(3-2)$ emission peaks, and averaged. The final spectra, with a total on-source integration time of 2.7 hours, are shown in Figure 1.

At 3 mm, we averaged all useful WILMA or FTS scans, after shifting them to a reference frequency of 102.756 GHz, and after removing bad channels from them. In contrast to the 1 mm data, the 3 mm data had signatures of standing waves due to the strong synchrotron continuum radiation, which increases with λ . We iteratively fitted the baseline of the WILMA data with sinusoidal functions of periods that are integer multiples of each other, representing different harmonics of the same standing wave. The best-fit solution that was indicated by the CLASS baseline routine corresponded to functions with periods of 0.28, 0.84, 1.68, and 2.52 GHz, and with an amplitude of 1 mK. These functions were removed from the WILMA spectrum, and

from the central part of the inner FTS spectrum¹. The final $^{12}\text{CO}(1-0)$ spectra, with a total on-source integration time of 1.2 hours, are shown in Figure 2. A similar approach was taken for the 2 mm data. A main-beam-temperature-to-flux conversion factor of 5.0 Jy K^{-1} was used to flux calibrate the final spectra at all wavelengths.

3. Results: CO in emission and in absorption

The $^{12}\text{CO}(3-2)$ profile of 4C12.50 consists of an emission component at systemic velocity, corresponding to a redshift of 0.1218, and of an absorption feature at approximately -1000 km s^{-1} from it. The $\text{CO}(2\rightarrow 3)$ absorption is seen in all four frequency tuning and backend combinations, indicating that the feature is intrinsic to the source. Its signal-to-noise (S/N) ratio is ~ 6 in both the WILMA and the FTS data, which have a corresponding root-mean-square noise of 1.7 mK and 1.8 mK, respectively. The outer FTS data provide further evidence that the absorption is real, as they rule out the existence of standing waves that could create a feature of this depth. With an absorption minimum at $30 (\pm 2) \text{ mJy}$ below the local $150 (\pm 20) \text{ mJy}$ continuum, the CO molecules are responsible for obscuring 20% of their 309.23 GHz background radiation. This corresponds to an observed optical depth at the center of the line, $\tau_{\text{obs},0}$, of $0.22 (\pm 0.05)$. Averaging the best Gaussian fit parameters to the data of each backend indicates that the minimum is at $-950 (\pm 90) \text{ km s}^{-1}$. The CO absorption profile remarkably resembles that of the HI absorption seen in

¹ A separate baseline fitting was not performed for the full FTS spectrum, as the combination of varying continuum levels and standing waves rendered this task uncertain.

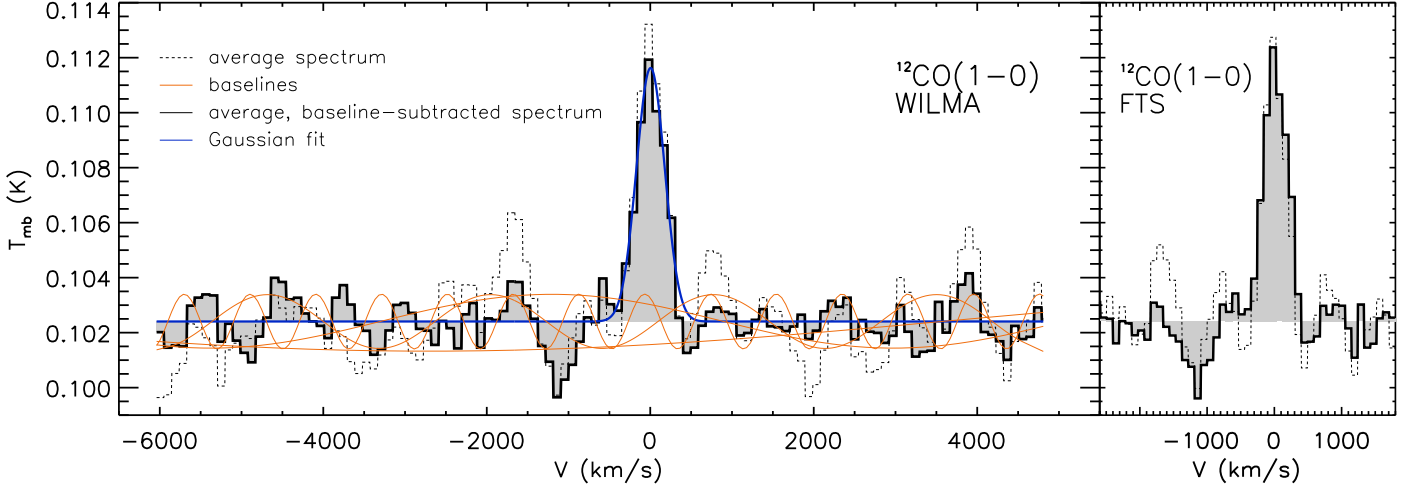


Fig. 2. WILMA (*left*) and FTS (*right*) $^{12}\text{CO}(1-0)$ spectrum of 4C12.50, binned to 93 km s^{-1} channels. The average spectrum prior to the removal of sinusoidal baselines, which represent the harmonics of a standing wave and which are shown in orange, is plotted with a dashed line. The final spectrum is shown as a solid, filled histogram.

radio data (Figure 1; Morganti et al., 2004). Its resolution-corrected width is $250 (\pm 80) \text{ km s}^{-1}$, reflecting the collective motions of multiple clouds along the line of sight.

An absorption line is also seen at -1100 km s^{-1} away from $^{12}\text{CO}(1-0)$ after the progressive subtraction of standing wave harmonics from the 3 mm baseline. However, the wave’s amplitude is comparable to the absorption’s minimum (Figure 2), impeding its exact profile study. We thus simply constrain $\tau_{\text{obs},0}(0 \rightarrow 1)$ towards the $0.51 (\pm 0.06) \text{ Jy}$ continuum background to an upper limit of 0.03.

The $^{12}\text{CO}(1-0)$ emission peaks at a main beam temperature of $9.2 (\pm 1.2) \text{ mK}$ above its underlying continuum. Its resolution-corrected width is $400 (\pm 95) \text{ km s}^{-1}$, and its intensity, $I_{\text{CO}(1-0)}$, is $4.0 (\pm 1.3) \text{ K km s}^{-1}$ (see Evans et al. 1999, 2005 for comparison). From this, we deduce that the cold H_2 gas reservoir of 4C12.50 is $1.0 (\pm 0.3) \times 10^{10} M_{\odot}$, assuming that the gas mass is given by the product $23.5 \alpha I_{\text{CO}(1-0)} \Omega_B D_L^2 / (1+z)^3 M_{\odot}$ (Solomon et al., 1997), where Ω_B is the telescope main beam area in arcsec^2 , D_L is the source luminosity distance in Mpc, and α is the CO luminosity to H_2 mass conversion factor. We used a telescope beam of $28''$ (61 kpc) at 103 GHz and an α value of $0.8 M_{\odot} (\text{K km s}^{-1} \text{ pc}^2)^{-1}$ (Downes & Solomon, 1998), because 4C12.50 has a ULIRG-like infrared luminosity of $2.5 \times 10^{12} L_{\odot}$.

The $^{12}\text{CO}(3-2)$ emission is detected with a S/N ratio of 25 and 21 in the WILMA and the FTS data, respectively. Its main beam temperature peaks at $17.5 (\pm 1.0) \text{ mK}$ above the local continuum. Its resolution-corrected width is $510 (\pm 65) \text{ km s}^{-1}$, and its intensity is $9.9 (\pm 1.6) \text{ K km s}^{-1}$.

The $I_{\text{CO}(3-2)} / I_{\text{CO}(1-0)}$ ratio, 2.5, is particularly below its theoretically predicted value in case of gas that is characterized by a single T_{ex} , 9, translating into a subthermal excitation for the ambient gas of 4C12.50. It is also below that of the central line of sight of M82, of several local AGN, ULIRGs, and radio galaxies, but above that of the outflow of M82, and similar to that of the Milky Way. This comparison is visualized in Figure 3 for the luminosity that each line carries. Even though this ratio is in itself indicative of large reservoirs of cold and diffuse gas, it does not rule out

the presence of a warm and dense, highly excited CO component for the ambient gas that can be revealed with high J CO emission lines. The non detection of HCN (or HCO^+) at a 3σ level of 0.86 K km s^{-1} for a width of 460 km s^{-1} cannot be used for or against either interpretation. It leads to a CO/HCN lower limit of 8 (Gao & Solomon, 2004) for a linearly interpolated $^{12}\text{CO}(2-1)$ intensity of 7 K km s^{-1} .

4. Discussion: on the properties of a multi-phase AGN-driven outflow

The rapid molecular gas motions provide direct evidence for the existence of an outflow in 4C12.50 because none of its merging components (Axon et al., 2000) is moving faster than $\pm 250 \text{ km s}^{-1}$ from systemic velocity (Holt et al., 2003; Rodríguez Zaurín et al., 2007). The maximum velocity of the gas, reaching -1500 km s^{-1} , is also atypical for supernova-driven outflows in starburst galaxies (e.g., Heckman et al., 2000; Rupke et al., 2005). It is instead characteristic of AGN-driven outflows (e.g., Rupke & Veilleux, 2011; Sturm et al., 2011). AGN radiation pressure and winds can affect the observed gas kinematics of 4C12.50: the AGN radiation does reach and ionize part of the outflowing gas, which contains Ne V and O IV ions (Spoon & Holt, 2009; Dasyra et al., 2011). The gas can also be pushed by shocks that were created as the radio jet of 4C12.50 (Stanghellini et al., 1997) propagated in the interstellar medium (ISM). An HI outflow in front of a bright radio knot (Morganti et al., 2004) makes this scenario plausible for the neutral gas, and even for the molecular gas. A jet-ISM interaction has been considered responsible for the irregular H_2 kinematics (Dasyra & Combes, 2011; Nesvadba et al., 2011), the strong H_2 emission (Ogle et al., 2010; Guillard et al., 2012), and the high CO excitation (Papadopoulos et al., 2008) in radio galaxies.

To constrain the CO column density along the line of sight, N_{CO} , from the observed absorption, we assume that the gas is homogeneously distributed and in local thermodynamic equilibrium (LTE). Its level populations then follow the Boltzmann distribution, and N_{CO} is related to the

optical depth through

$$N_{\text{CO}} = 8\pi \frac{\nu^3}{c^3} \frac{Q(T_{\text{ex}}) e^{E_J/kT_{\text{ex}}}}{g_{J+1} A_{J+1,J} (1 - e^{-h\nu/kT_{\text{ex}}})} \int \tau dV \quad (1)$$

(e.g., Wiklind & Combes, 1995), where c is the lightspeed, h is the Planck constant, k is the Boltzmann constant, E_J and g_J are the energy and the statistical weight of the state J , respectively, $A_{J+1,J}$ is the Einstein coefficient for spontaneous emission, ν is the frequency of the emitted line, and Q is the partition function at the excitation temperature T_{ex} . The ratio $\int \tau(2 \rightarrow 3) dV / \int \tau(0 \rightarrow 1) dV$ agrees with its observed limit, >6.4 , if $T_{\text{ex}} \geq 65$ K. This points to high turbulence in the gas, to which shocks could contribute through collisions. For $T_{\text{ex}}=65$ K, N_{CO} is equal to $1.8 \times 10^{18} \text{cm}^{-2}$.

This number will increase with increasing T_{ex} , but it will remain in the same order of magnitude up to 200 K. The filling factor of the background source by the molecular clouds, f_c , can play an important role in the T_{ex} and N_{CO} determination. Partial coverage of the background source ($f_c < 1$) will make the observed (beam-averaged) optical depth deviate from its actual value, which will then be equal to $-\ln[1 - (1 - e^{-\tau_{\text{obs}}})/f_c]$ (Wiklind & Combes, 1994). This relation is computed from the radiative transfer equation, assuming that the gas is in LTE, that $T_{\text{ex}} \ll T_{\text{bg}}$, and that the cosmic microwave background contribution to the gas excitation is negligible (e.g., Staguhn et al., 1997). Requiring the gas to be optically thick limits f_c to values above 0.2. Data of multiple transitions are needed to further constrain the column density, permitting f_c to be measured, and large velocity gradients (Scoville & Solomon, 1974) and different energy level populations (e.g., Goldsmith, 1972; Israel et al., 1991) to be examined.

For the present assumptions and for a standard CO-to-H₂ abundance ratio of 10^{-4} , the H₂ column density, N_{H_2} , is $\gtrsim 2 \times 10^{22} \text{cm}^{-2}$. The HI column density towards the outflow is estimated to be $3 \times 10^{21} \text{cm}^{-2}$ based on both optical NaI data (Rupke et al., 2005) and radio HI data (Morganti et al., 2005, for $T_{\text{spin}}=1000$ K). For the ambient HI gas at systemic velocity, which is located 100 pc north-west of the radio core, the column density is $6 \times 10^{20} \text{cm}^{-2}$ – 10^{22}cm^{-2} (Morganti et al., 2004; Curran & Whiting, 2010, for $T_{\text{spin}}=100$ K). The largest uncertainty in this comparison is the wavelength-dependent spatial distribution of the background and the foreground source. The radio core emission typically dominates the mm and even the submm (850 μm ; Clements et al. 2010) continuum, because the emission from diffuse jet knots is described by a steep power law that fades fast with frequency (Krichbaum et al., 1998, 2001, 2008). We thus assume the mm background area to be spatially constrained within the 2 cm beam.

For a beam area of 3 milliarcsec² (Lister et al., 2003) and $N_{\text{H}_2}=1.8 \times 10^{22} \text{cm}^{-2}$, we find that the outflow entrains $4.2 \times 10^3 M_{\odot}$ of cold H₂ gas in front of the mm core of 4C12.50. How this mass compares with the mass of the cold H₂ gas that flows over all lines of sight remains unclear. It is therefore unknown if the outflow carries less cold than warm H₂ gas. However, the outflowing-to-ambient mass ratio of the cold gas will be lower than that of the 400 K gas (37%; Dasyra & Combes 2011), as long as the cold outflowing gas weighs less than $3 \times 10^9 M_{\odot}$. If this amount of gas existed in the mm beam, and without a background source illuminating most of the clouds, the outflow would be seen in emission. Instead, our ¹²CO(0 → 1) data limit any further

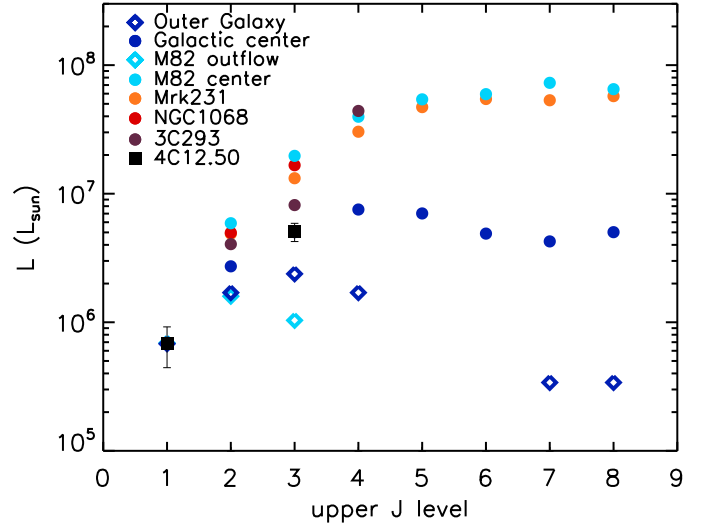


Fig. 3. Luminosities of CO lines in 4C12.50 and other sources. A normalization factor of $L_{\text{CO}(1-0)}(4\text{C12.50})/L_{\text{CO}(1-0)}$ has been applied to the line luminosities of all other sources. The data are from Fixsen et al. (1999); Dumke et al. (2001); Weiss et al. (2001, 2005); Papadopoulos et al. (2007, 2008); Panuzzo et al. (2010); van der Werf et al. (2010); Krips et al. (2011). Typical uncertainties for the ancillary data are 0.1–0.3 dex.

outflowing cold gas mass to an upper value of $2 \times 10^9 M_{\odot}$ when integrating over a 1500km s^{-1} velocity range and over a 1000kpc^2 area (Batcheldor et al., 2007).

5. Summary

We present deep 30 m observations of ¹²CO (1–0) and (3–2) in the nearby ULIRG/radio galaxy 4C12.50, which is known to have an impressive outflow entraining more than $\sim 1/4$ th of its warm, 400 K H₂ gas (Dasyra & Combes, 2011). Our observations led to the discovery of the cold component of the molecular outflow. Absorption from J=2→3 is seen in data that were obtained with two different central frequency tunings and backends. It peaks at -950km s^{-1} from systemic velocity. Its profile resembles that of the HI absorption component that traces the neutral gas outflow (Morganti et al., 2004). Absorption is also potentially discovered in the 0→1 transition. Treating the optical depth of the latter as an upper limit and assuming that the molecular clouds fully cover their background source, we find that the molecular gas is turbulent, with an excitation temperature of at least 65 K in LTE conditions. For this temperature, the H₂ column density is $1.8 \times 10^{22} \text{cm}^{-2}$. It suggests that the outflow carries $4.2 \times 10^3 M_{\odot}$ of cold H₂ gas along the nuclear line of sight. Even if the mass of the cold outflowing gas could exceed that of the warm outflowing gas, $5.2 \times 10^7 M_{\odot}$, for a higher N_{CO} value or when integrating over several lines of sight, it would most likely not exceed $3 \times 10^9 M_{\odot}$, i.e., 1/3rd of the ambient cold gas reservoir. The outflowing-to-ambient mass ratio could thus be elevated in the warm gas phase with respect to the cold gas phase.

Acknowledgements. K. D. acknowledges support by the Centre National d’Etudes Spatiales (CNES), and is thankful to P. Salomé for technical tips and to P. Papadopoulos for useful discussions. Based on data obtained with the 30 m telescope of IRAM, which is supported by INSU/CNRS (France), MPG (Germany) and IGN (Spain).

References

- Aalto, S., Garcia-Burillo, S., Muller, S., et al. 2012, *A&A*, 537, 44
- Axon, D. J., Capetti, A., Fanti, R., et al. 2000, *AJ*, 120, 2284
- Batcheldor, D., Tadhunter, C., Holt, J., et al. 2007, *ApJ*, 661, 70
- Booth, C. M., & Schaye, J. 2009, *MNRAS*, 398, 53
- Clements, D. L., Dunne, L., & Eales, S. 2010, *MNRAS*, 403, 274
- Croton, D. J., Springel, V., White, S. D. M., et al., 2006, *MNRAS*, 367, 864
- Curran, S. J., & Whiting, M. T. 2010, *ApJ*, 712, 303
- Dasyra, K. M., Ho, L. C., Netzer, H., et al. 2011, *ApJ*, 740, 94
- Dasyra, K. M., & Combes, F. 2011, *A&A*, 533, L10
- Debuhr, J., Quataert, E., & Ma, C.-P. 2012, *MNRAS*.tmp.2150
- Downes, D., & Solomon, P. M. 1998, *ApJ*, 507, 615
- Dumke, M., Nieten, Ch., Thuma, G., Wielebinski, R., & Walsh, W. 2001, *A&A*, 373, 853
- Evans, A. S., Mazzarella, J. M., Surace, J. A., et al. 2005, *ApJS*, 159, 197
- Evans, A. S., Kim, D. C., Mazzarella, J. M., Scoville, N. Z., & Sanders, D. B. 1999, *ApJ*, 521, L107
- Feruglio, C., Maiolino, R., Piconcelli, E., et al. 2010, *A&A*. 518. L155
- Fischer, J., Sturm, E., González-Alfonso, E., et al. 2010, *A&A*, 518, L41
- Fixsen, D. J., Bennett, C. L., & Mather, J. C. 1999, *ApJ*, 526, 207
- Gao, Yu, & Solomon, P. M. 2004, *ApJ*, 606, 271
- Goldsmith, P. F. 1972, *ApJ*, 176, 597
- Guillard, P., Ogle, P., Emonts, B., et al. 2012, *ApJ*, in press (arXiv/1201.1503)
- Heckman, T. M., Lehnert, M. D., Strickland, D. K., & Armus, L. 2000, *ApJS*, 129, 493
- Holt, J., Tadhunter, C. N., & Morganti, R. 2003, *MNRAS*, 342, 227
- Hopkins, P. F., & Elvis, M. 2010, *MNRAS*, 401, 7
- Israel, F. P., van Dishoeck, E. F., Baas, F., de Graauw, T., & Phillips, T. G. 1991, *A&A*, 245, L13
- Krichbaum, T. P., Alef, W., Witzel, A., et al., 1998, *A&A* 329, 873
- Krichbaum, T. P., Graham, D. A., Witzel, A., et al. 2001, *ASPC*, 250, 184
- Krichbaum, T. P., Lee, S. S., Lobanov, A. P., Marscher, A. P., & Gurwell, M. A. 2008, *ASPC*, 386, 186
- Krips, M., Martn, S., Eckart, A., et al. 2011, *ApJ*, 736, 37
- Lister, M. L., Kellermann, K. I., Vermeulen, R. C., et al. 2003, *ApJ*, L584, 135
- Morganti, R., Oosterloo, T. A., Tadhunter, C. N., et al. 2004, *A&A*, 424, 119
- Morganti, R., Tadhunter, C. N., & Oosterloo, T.A., 2005, *A&A* 444, L9
- Nesvadba, N. P. H., Boulanger, F., Lehnert, M. D., Guillard, P., & Salomé, P. 2011*A&A*, 536, L5
- Ogle, P., Boulanger, F., Guillard, P., 2010, *ApJ*, 724, 1193
- Panuzzo, P., Rangwala, N., Rykala, A., et al. 2010, *A&A*, 518, L37
- Papadopoulos, P. P., Isaak, K. G., & van der Werf, P. P. 2007, *ApJ*, 668, 815
- Papadopoulos, P. P., Kovacs, A., Evans, A. S., & Barthel, P. 2008, *A&A*, 491, 483
- Rodríguez Zaurín, J., Holt, J., Tadhunter, C. N., & González Delgado, R. M. 2007, *MNRAS*, 375, 1133
- Rupke, D. S., Veilleux, S., & Sanders, D. B. 2005, *ApJ*, 632, 751
- Rupke, D. S. N., & Veilleux, S. 2011, *ApJ*, 729, L27
- Sijacki, D., Springel, V., Di Matteo, T., Hernquist, L. 2007, *MNRAS*, 380, 877
- Scoville, N. Z., & Solomon, P. M. 1974, *ApJ*, 187, L67
- Solomon, P. M., Downes, D., Radford, S. J. E., & Barrett, J. W. 1997, *ApJ*, 478, 144
- Spoon, H. W. W., & Holt, J. 2009, *ApJ*, 702, L42
- Staguhn, J., Stutzki, J., Chamberlin, R. A., et al. 1997, *ApJ*, 491, 191
- Stanghellini, C., O’Dea, C. P., Baum, S. A., et al. 1997*A&A*, 325, 943
- Sturm, E., González-Alfonso, E., Veilleux, S., et al. 2011, *ApJ*, 733, L16
- van der Werf, P. P., Isaak, K. G., Meijerink, R., et al. 2010, *A&A*, L518, 42
- Weiss, A., Neininger, N., Hüttemeister, S., & Klein, U. 2001, *A&A*, 365, 571
- Weiss, A., Walter, F., & Scoville, N. Z. 2005, *A&A*, 438, 533
- Wiklind, T. & Combes, F. 1994, *A&A*, 286, L9
- Wiklind, T. & Combes, F. 1995, *A&A*, 299, 382